Partitioning of solutes in multiphase Ti–Al alloys

R. Benedek, A. van de Walle, S. S.A. Gerstl, M. Asta, and D. N. Seidman
Department of Materials Science and Engineering, Northwestern University, Evanston, Illinois 60208, USA

C. Woodward
Department of Materials Science and Engineering, Northwestern University, Evanston, Illinois 60208, USA
and Air Force Research Laboratory, Materials and Manufacturing Directorate, Wright Patterson AFB, Ohio 45433-7817, USA
(Received 9 September 2004; revised manuscript received 1 December 2004; published 4 March 2005)

First-principles calculations based on a plane-wave pseudopotential method, as implemented in the VASP code, are presented for the formation energies of several transition-metal and non-transition-metal dopants in Ti–Al alloys. Substitution for either Ti or Al in γ-TiAl, α_2-Ti_3Al, Ti_2AlC, and Ti_3AlC are considered. Calculated (zero-temperature) defect formation energies exhibit clear trends as a function of the periodic-table column of transition metal solutes. Early transition metals in TiAl prefer the Ti sublattice, but this preference gradually shifts to the Al sublattice for late transition metals; the Ti sublattice is preferred by all transition metal solutes in Ti_3Al. Partitioning of solutes to Ti_3Al is predicted for mid-period transition elements, and to TiAl for early and late transition elements. A simple Ising model treatment demonstrates the plausibility of these trends, which are in excellent overall agreement with experiment. The influence of temperature on formation energies is examined with a cluster expansion for the binary TiAl alloys and a low temperature expansion for dilute ternary alloys. Results for Nb-doped alloys provide insight into the relative sensitivity of solute partitioning to individual contributions to the free energy. Whereas the calculated formation energy of Nb (substitution) at zero temperature favors partitioning to α_2-Ti_3Al, temperature-dependent contributions to the formation free energy, evaluated at 1075 K, favor partitioning to γ-TiAl, in agreement with experiment.

DOI: 10.1103/PhysRevB.71.094201 PACS number(s): 61.66.Dk, 64.75.+g

I. INTRODUCTION

Light weight, high strength, and corrosion resistance make multiphase TiAl alloys[1] attractive materials for high-temperature structural applications, particularly in the automotive and aerospace industries.[2] In spite of these intrinsic advantages, issues such as room-temperature brittleness,[3] only moderate creep resistance,[4,5] the development of optimal anticorrosion coatings,[6] optimal processing methods,[7] and stability in low *p*H environments[8] must be addressed before TiAl can be put into wider service. Although the tantalizing prospect of the replacement of Ni-based superalloys by TiAl in high-pressure turbine components now seems unlikely,[9] titanium aluminides are nevertheless expected to continue to be technologically important structural alloys.

Dopants are often introduced into TiAl-alloy prototypes to improve their properties and performance. The selection of micro-alloying components has been guided primarily by empiricism. The detailed distribution of these dopants, as well as their influence on microscopic mechanisms that bear on materials properties, is poorly understood. Several types of solute behavior may be envisaged. Some solutes, such as C,[10,11] N,[10] B, and Si, form precipitates, whereas others form solid solutions in the host phases, from which they may preferentially segregate to defects and the heterophase interfaces in the system. Accurate information on the distribution of the solutes derived from simulation would be valuable for the future design and optimization of titanium-aluminide-based materials. The focus of this article is on bulk solute behavior. Some of our preliminary work on pristine interfaces of TiAl with carbides was published recently.[12]

Formation energies for point defects, either intrinsic or extrinsic, in metallic systems are typically much larger than thermal energies ($\sim k_BT$), and calculated defect energies at zero temperature are often sufficient for most purposes. In the case of Ti–Al alloys, however, the effect of temperature on defect energies merits careful attention. For example, the differences in formation energy for a solute in different phases, or on different sublattices in a given phase, are generally much smaller than individual formation energies and may be comparable to k_BT in some cases.[13] Moreover, the phase boundaries for the two-phase (γ, α_2) region of interest shift appreciably at elevated temperatures, driven by chemical potential changes that can also dramatically alter the relevant defect energies.

Several applications of first-principles methods to predict point-defect concentrations in intermetallic compounds have appeared.[14–16] In these treatments, point-defect energy parameters derived from first-principles calculations are combined with Bragg-Williams (lattice-gas) model analyses of configurational entropy to predict the equilibrium concentrations of defects as a function of stoichiometry and temperature. Along similar lines, the site preferences for selected solutes in γ-TiAl have been predicted by combining first-principles calculations with a multi-component lattice-gas model.[13]

Such treatments have thus far been restricted to a single alloy phase, and the consequences of a two-phase equilibrium for defect properties have not been explored. Many aspects of the analysis of defects in single-phase systems carry over to two-phase systems; in the latter, however, we require the chemical potentials of Ti and Al appropriate to compositions within the two-phase region. The chemical potentials in this region are, of course, closely related to the equilibrium-phase-diagram boundaries.

Several simulations of the phase diagram of binary Ti–Al have been published. Asta and co-workers used the cluster variation method to study phase stability for hcp and fcc phases.[17] More recently, van de Walle and co-workers re-evaluated the Ti-rich region of the Ti–Al phase diagram using Monte Carlo simulation based on a cluster expansion,[18] and included vibrational and electronic as well as configurational entropy.

In this paper we investigate solute partitioning among bulk titanium aluminide phases γ-TiAl and α_2-Ti_3Al and carbide-precipitate phases Ti_2AlC and Ti_3AlC. We focus particularly on the two-phase region, in which TiAl and Ti_3Al are in equilibrium, which is the composition range of greatest practical interest.[1] We calculate the relevant energy parameters for solutes in these phases within the generalized-gradient approximation of local-density-functional theory (LDFT-GGA). The solutes treated include most elements from transition groups IIIA to VIIIA, as well as B and Si.

Considerable simplification of the theory occurs in the limits of dilute solute concentrations and zero temperature. Although these limits are not relevant to most technological applications of Ti–Al alloys, the corresponding predictions represent a useful benchmark, and most of the results presented in this article will pertain to the zero-temperature dilute-solute limit. As touched upon earlier, however, a more comprehensive perspective is only possible with an understanding of how defect properties are modified at elevated temperatures. Therefore, we give considerable attention in this article to the calculation of the influence of temperature on solute formation energies. In our finite temperature calculations, however, we continue to resort to the dilute solute limit. The effects of solute-solute interactions and solute-induced shifts in the phase boundaries, for example, are thereby excluded. Although such effects are not necessarily insignificant for practical dopant levels that may individually extend to several percent, and in the presence of several different solutes, it appears logical to address the dilute limit first.

We employ a cluster expansion method[18] to calculate the free energy of the Ti–Al binary alloy as a function of host composition and temperature. This approach enables phase boundaries and chemical potentials of the binary system to be determined. The effects of ternary (solute) elements are treated in the dilute limit with a low-temperature expansion. Nb, a commonly employed dopant with a wide solubility range, is selected as a representative solute in TiAl.[19] Owing to the extensive calculations required to evaluate the temperature-dependent contributions to the solute formation free energy, only Nb is considered here.

In our low-temperature calculations, we find that, for group VA solutes and at least one group VIA solute, the difference between formation energies on the Ti and Al sublattices of γ-TiAl is of the order of a couple of tenths of an eV. Similarly, the difference between formation energies in the α_2 phase and in the γ phase is small for several solutes. At low temperatures, Nb is predicted to favor the α_2 phase. However, at elevated temperatures, Nb is predicted to switch preference to the γ phase, in agreement with experiment. In general, when the difference between the formation energies in the two phases is relatively small (of the order of a tenth of an eV), thermal corrections to the formation free energies cannot automatically be assumed insignificant.

The calculated formation energies at zero temperature for transition metals in the different phases show pronounced trends (albeit with some scatter) across the periodic table. For example, the sublattice preference of solutes in TiAl shifts from the Ti sublattice in the early transition metals to the Al sublattice in late transition elements, whereas the Ti sublattice is preferred uniformly for solutes in Ti_3Al. Further, solutes in the middle of a transition series partition to Ti_3Al, whereas only early and late transition metals prefer TiAl. The effects of temperature on the formation free energies are too weak to significantly perturb these trends. Some of the trends are captured by a simple Ising-type interaction model, which lends additional credibility to the results. Close agreement of the predicted trends with experiment is found, where comparison is possible.

II. SOLUTE FORMATION ENERGIES AND FREE ENERGIES

The partitioning of dilute concentrations of solutes among the phases of the alloy at thermal equilibrium is determined by their relative formation energies (or free energies) in those phases. We evaluate in this work the formation energies of solute species of interest in the host titanium-aluminide phases γ-TiAl and α_2-Ti_3Al, and in carbide precipitate phases. The formation energy of species i on sublattice j of phase β may be written as[20]

$$E_F(i,j,\beta) = \Delta E(i,j,\beta) - \Delta(N\mu), \tag{1}$$

where ΔE is the cohesive energy change upon substitution of an i atom for a host atom on the j sublattice of phase β, and $\Delta(N\mu)$ accounts for the chemical potentials of atoms added or removed from thermodynamic reservoirs during the formation of the defect. Thus, for a substitutional solute, $\Delta(N\mu) = \mu(i) - \mu(k_{\beta_j})$, where k_{β_j} denotes the atomic species on sublattice j of phase β. $\Delta E(i,j,\beta)$ is evaluated with the lattice surrounding the solute relaxed to equilibrium.

This formulation of the solute formation energy is applicable at zero temperature, and at ideal host stoichiometry, when the atomic species, k_{β_j}, that occupies each sublattice is unique. At elevated temperatures, the formulation should be generalized to the case of partial occupancy, and corrected for lattice expansion and thermal disorder, as well as shifts in the phase boundaries of γ-TiAl and α_2-Ti_3Al and host chemical potentials. The formation energy, $E_F(i,j,\beta,T)$, is thus temperature dependent. Vibrational entropy contributions $TS_F^{\mathrm{vib}}(i,j,\beta,T)$ to the free energy[21,22] also become significant at elevated temperatures.

Formally, the equilibrium concentration of impurity species i is related to the derivative of the thermodynamic potential with respect to its chemical potential.[20] In the dilute limit, this concentration is exponentially related to the thermodynamic free energy of formation,

$$\Omega_F(i,j,\beta,T) = E_F(i,j,\beta,T) - TS_F^{\mathrm{vib}}(i,j,\beta,T):$$
$$c(i,j,\beta,T) = \exp[-\Omega_F(i,j,\beta,T)/k_BT]. \tag{2}$$

Although Eq. (2) is well established for stoichiometric com-

pounds, its applicability to alloys with appreciable deviations from stoichiometry has apparently not been discussed. The Appendix of this paper shows that Eq. (2) holds for the case of dilute ternary additions to binary compounds with concentrated antisite disorder, provided the defect formation free energy is defined as a configurational average.

III. NUMERICAL RESULTS

First-principles calculations of total energies are performed within the generalized-gradient-approximation (GGA)[23] of density functional theory, as implemented in the VASP code.[24] The calculations employ a plane-wave basis combined with the ultrasoft pseudopotential formalism.[25] Calculations are performed for four different phases, γ-TiAl and α_2-Ti_3Al, as well as the carbides Ti_2AlC (H-type) and Ti_3AlC (P-type). Special k-point sets based on Monkhorst-Pack[26] indices (888) are employed. In all of the calculations for cells with defects (intrinsic point defects or solute atoms), the internal coordinates are relaxed to equilibrium, as mentioned above.

In principle, of course, the cell dimensions (lattice constants) also relax in the presence of point defects. This correction, however, is often negligible in practice for periodic supercells of metallic systems with a few dozen atoms or more. A test calculation was performed for an Al vacancy in a 32-atom γ-TiAl cell; similar volume-relaxation energies are anticipated for the 64-atom cell employed for the α_2 phase. The equilibrium volume in the presence of the Al vacancy in TiAl decreased by about 1%, relative to that for the defect-free crystal, and the total energy of the cell decreased by about 0.025 eV, relative to that obtained at the defect-free crystal equilibrium volume. The influence of volume relaxation on point defect energies for solutes is expected to be of similar magnitude to that for vacancies, or smaller. Energy changes of this magnitude are small relative to the scale of most of the energies calculated in this work; the effects of such volume-relaxation energies on trends is expected to be especially small, because of cancellations. The results presented in the remainder of this article correspond to cells in which the volumes are fixed at the equilibrium values for the ideal stoichiometries.

A. Host material lattice constants

Calculations for tetragonal $L1_0$ γ-TiAl utilized a 32-atom cell, which corresponds to doubling the lattice constants of the conventional face-centered-tetragonal unit cell. Equilibrium lattice constants (in Angstrom units) $a=7.96/2=3.98$ (experiment: 4.005), and $c=8.182/2=4.09$ (experiment: 4.07), were obtained. Calculations for hexagonal $D0_{19}$ α_2-Ti_3Al were based on a 64-atom cell, obtained by doubling the hexagonal-layer lattice constants, as well as the lattice constant perpendicular to the layers. The predicted equilibrium lattice constants are $a=11.50/2=5.75$ (experiment: 5.78) and $c=9.304/2=4.652$ (experiment: 4.64). Calculations for Ti_2AlC, a hexagonal system, were based on a 64-atom cell obtained by doubling the hexagonal-layer lattice constants and the c-axis lattice constant. The predicted equilibrium lattice constants are $a=6.14/2=3.07$ (experiment: 3.04) and $c=27.384/2=13.69$ (experiment: 13.623). Calculations for Ti_3AlC, a cubic perovskite, were based on a 40-atom cell obtained by doubling the cubic lattice constant. The predicted equilibrium lattice constants are $a=8.36/2=4.18$ (experiment: 4.156).

For the first three of these structures, a is slightly underestimated and c (and therefore c/a) is slightly overestimated, which is often found for layered or tetragonal systems within the LDFT-GGA.

B. Chemical potentials

The defect formation energy, Eq. (1), depends on the chemical potentials of the host elements Ti and Al. Of particular interest are compositions within the two-phase region in which TiAl and Ti_3Al are in equilibrium. If the formation energies of intrinsic point defects, i.e., vacancies, interstitials, and antisite atoms, are positive, the chemical potentials at zero temperature μ(Ti) and μ(Al) satisfy the relations

$$\mu(\mathrm{Ti}) + \mu(\mathrm{Al}) = \mu(\mathrm{TiAl}), \tag{3}$$

and

$$3\mu(\mathrm{Ti}) + \mu(\mathrm{Al}) = \mu(\mathrm{Ti_3Al}), \tag{4}$$

where μ(TiAl) and $\mu(Ti_3Al)$ are the cohesive energies, per formula unit, of the two phases. VASP supercell calculations yield $\mu(\mathrm{TiAl})=-12.242$ eV and $\mu(Ti_3Al)=-27.993$ eV from which we obtain $\mu(\mathrm{Ti})=-7.876$ eV and $\mu(\mathrm{Al})=-4.367$ eV.

The assumption of positive intrinsic defect formation energies may be verified *a posteriori*, based on these chemical potentials.

C. Intrinsic point defect energies

Intrinsic defect formation energies can be expressed in terms of $\Delta E(i,j,\beta)$, the difference between the total energy of a computational unit cell with a vacancy or an antisite atom, and the energy of a defect-free reference cell. Thus,

$$E_F(v,j,\beta,0) = \Delta E(v,j,\beta) - \mu(j) \tag{5}$$

is the vacancy formation energy on sublattice j of phase β at zero temperature, where $\mu(j)$ is the chemical potential of the atomic species on sublattice j. Similarly,

$$E_F(\overline{j},j,\beta,0) = \Delta E(i,j,\beta) - \mu(i) + \mu(j) \tag{6}$$

is the formation energy of an antisite atom (substitution onto sublattice j of an atom of the species on sublattice $\overline{j}$), where $\overline{j} \neq j$. Numerical results for both vacancies and antisite atoms are listed in Table I. Since the defect energies are all positive, the ideal compound stoichiometries of TiAl and Ti_3Al are stable at low temperatures. This is in contrast to the behavior at elevated temperatures,[27] at which the phase boundary of the α_2 phase corresponds approximately to Ti_2Al rather than Ti_3Al.

We observe in Table I that the formation energies of vacancies on either sublattice of TiAl or Ti_3Al are considerably larger than those of antisite atoms, which indicates that de-

TABLE I. Formation energies of intrinsic defects in two-phase ($TiAl, Ti_3Al$) region.

Phase	E_F^V(Ti)	E_F^V(Al)	E_F^a(Ti)	E_F^a(Al)
TiAl	1.76	1.97	0.30	0.70
Ti_3Al	3.15	2.76	0.54	0.16

viations from stoichiometry at most temperatures are accommodated primarily by antisite atoms, and the number of vacancies in thermal equilibrium is quite small.

D. Solute formation energies

The solute formation energy

$$E_F(i,j,\beta,0) = \Delta E(i,j,\beta) - \mu(i) + \mu(j), \tag{7}$$

where i refers to the solute species. The phases under consideration are labeled $\beta=\gamma$ for TiAl, $\beta=\alpha_2$ for Ti_3Al, $\beta=$H for Ti_2AlC, and $\beta=$P for Ti_3AlC.

The relative formation energy of a given solute i in phases β_1 and β_2,

$$\Delta E_F(i) = E_F(i,j_1,\beta_1,0) - E_F(i,j_2,\beta_2,0), \tag{8}$$

is independent of the solute chemical potential, $\mu(i)$. We require only that its value be consistent with the assumption of diluteness. Incidentally, knowledge of the solute chemical potential is necessary to predict absolute solubility in a given phase,[28] which is not addressed in this article.

Once the host chemical potentials are known, the chemical potential for carbon can be obtained from the total energy of the carbide:

$$\mu(\mathrm{C}) = \mu(\mathrm{Ti_2AlC}) - 2\mu(\mathrm{Ti}) - \mu(\mathrm{Al}), \tag{9}$$

where $\mu(Ti_2AlC)$ is the total energy of the H-phase per formula unit. An almost identical value of μ(C) is obtained from the energy of the P-phase, Ti_3AlC. [We note, incidentally, that Eqs. (3), (4), and (9) do not imply vanishing compound heats of formation, because the chemical potentials μ(Ti) and μ(Al) correspond to the two-phase region rather than to the respective elemental materials.]

1. Solute sublattice preference in host phases

The differences between the formation energies of solutes on the $j_1=$Al and $j_2=$Ti sublattices in the $\beta=\gamma$ and $\beta=\alpha_2$ phases,

$$\Delta E_F(i,0) = E_F(i,j_1,\beta,0) - E_F(i,j_2,\beta,0), \tag{10}$$

are plotted in Fig. 1. The ordinate represents $\Delta E_F(i)$ and the abscissa the periodic-table column of the solute. For groups where more than one member is considered (e.g., Cr, Mo, and W in group VIA), the members are offset from each other in intervals of 0.1 (for example, Cr: 5.9, Mo: 6.0, W: 6.1). A preference for the Ti sublattice in TiAl occurs for early transition metal solutes, whereas the later transition metals increasingly prefer the Al sublattice. This variation across the periodic table is in contrast to solute behavior in Ti_3Al, in which the Ti sublattice is preferred by all solutes.

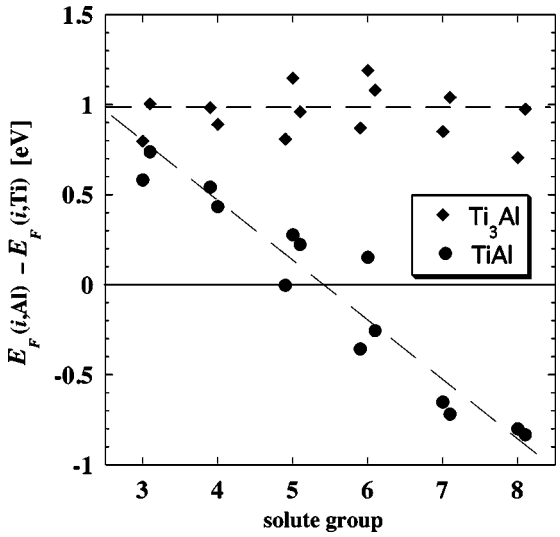

FIG. 1. Difference between the formation energies for solute substitution on the Al sublattice and on the Ti sublattice of TiAl (filled circles) and Ti_3Al (filled diamonds). Results are shown for selected solutes in the transition metal series IIIB–VIIIB. The nontransition elements Si and B (not represented in the plot) strongly favor the Al sublattice in both phases. The abscissa value is shifted slightly to enable members of the same group to be distinguished, e.g., Cr: 5.9, Mo: 6.0, W: 6.1. The trends in the data indicate that the Al sublattice in TiAl is increasingly preferred for the later transition groups. The crossover between Ti preference and Al preference occurs roughly between groups VB and VIB. Transition metal solutes in Ti_3Al all prefer the Ti sublattice.

Although the trends exhibited in Fig. 1 are clear, a fair amount of scatter is found for the TiAl phase, particularly for different members of groups VA and VIA. For these groups, the formation energies on the Ti and Al sublattices of TiAl are fairly comparable. Solutes with small $\Delta E_F(i)$ (<0.1 eV, approximately) are shared between the two sublattices.[13] The lack of a strong sublattice preference makes the temperature-dependent contributions to the formation free energies of particular interest for these groups. Temperature-dependent contributions to the formation free energy of Nb are presented below.

Results for the nontransition element solutes B and Si, analogous to those plotted in Fig. 1, show that substitution on the Al sublattice is preferred by both in either aluminide phase. The energy differences between the two sublattices for these solutes is in the range 0.8 to 1.0 eV.

2. Solute partitioning

We consider next the relative formation energies of solutes in TiAl and Ti_3Al. We plot in Fig. 2 the difference

$$\Delta E_F^{\alpha_2\gamma}(i) = E_F(i,j_{\alpha_2},\alpha_2,0) - E_F(i,j_\gamma,\gamma,0), \tag{11}$$

where j_{α_2} denotes the preferred sublattice of solute i in the α_2-phase and j_γ the preferred sublattice in the γ phase. A negative value of $\Delta E_F^{\alpha_2\gamma}(i)$ signifies that the α_2 phase is preferred. Almost all solutes considered prefer the α_2 phase, the

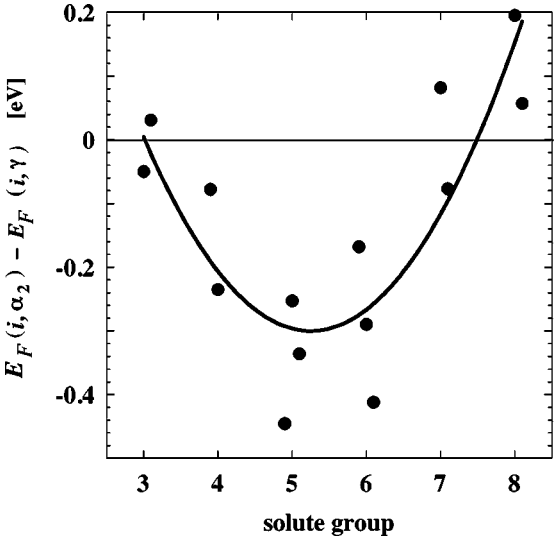

FIG. 2. Difference between the formation energies for solute substitution in Ti_3Al and TiAl for selected solutes in the transition metal series IIIB–VIIIB. The formation energy that corresponds to the preferred sublattice (cf. Fig. 1) for each phase is employed. Apart from a few early (Y) and late (Mn,Ru) transition metals, a distinct preference for the Ti_3Al phase is observed.

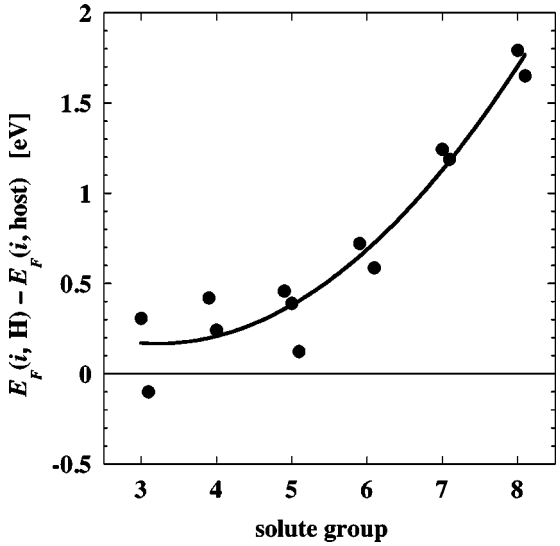

FIG. 3. The difference between the formation energies for solute substitution in the preferred carbide (Ti_2AlC or Ti_3AlC) and in the aluminide host (either Ti_3Al or TiAl, whichever has the lower energy).

exceptions being the early transition metal Y and the late transition metals Mn, Fe, and Ru, which have only a slight preference for the γ phase. Groups VB and VIB show a particularly strong preference for α_2.

Nontransition elements are predicted to partition to the α_2 phase: $\Delta E_F^{\alpha_2\gamma}(i) = -0.3$ for B, and -0.6 eV for Si.

3. Solute formation energies in carbides

Transition metal solutes in the H- and P-type carbides substitute primarily on the Ti sublattice. An exception is the group IIIB element Y in the H-type carbide, which substitutes on the Al sublattice. In Fig. 3 we plot the difference between the lowest formation energy of solutes in the H-type carbides and the lowest formation energy in the host phases. Negative values indicates a preference for carbide over host. Of the two carbides, the H-type carbide is preferred by all transition metal solutes except Sc. In Fig. 3, only Y shows a negative relative formation energy; we note that Sc has a relative formation energy close to zero, with respect to the P-type carbide (not shown in plot). The trend of later transition metal groups is to favor the host phases over carbides by increasing amounts.

E. Temperature dependence

Since service temperatures of interest for titanium aluminides extend to 800–1000 °C (about 60% to 70% of the melting temperature) and processing temperatures are somewhat higher, the behavior of defect properties in these temperature ranges would be of interest. Nb was selected for investigation, because a relatively marginal phase preference for this solute was found in zero temperature calculations, and finite-temperature corrections may therefore be required to get qualitatively correct results. Results will be reported for a temperature of 1075 K.

Let us consider the free energy of formation for a solute atom, $\Omega_F(i,j,\beta,T)$. At zero temperature, $\Omega_F(i,j,\beta,0) = E_F(i,j,\beta,0)$. We express the temperature correction to the formation free energy, $\Delta\Omega_F(i,j,\beta,T) = \Omega_F(i,j,\beta,T) - \Omega_F(i,j,\beta,0)$, as $\Delta\Omega_F(i,j,\beta,T) = \Delta\Omega_F^h(i,j,\beta,T) + \Delta\Omega_F^t(i,j,\beta,T) + \Delta\Omega_F^\mu(i,j,\beta,T) + \Delta\Omega_F^{stoi}(i,j,\beta,T)$.

$\Delta\Omega_F^h(i,j,\beta,T)$ is the vibrational free energy of defect formation obtained within the harmonic approximation, whereas $\Delta\Omega_F^t(i,j,\beta,T)$ is the contribution of thermal expansion to the vibrational free energy. $\Delta\Omega_F^\mu(i,j,\beta,T)$ represents the change in defect formation energy that results from the temperature dependence of the chemical potentials within the two-phase region. Finally, $\Delta\Omega_F^{stoi}(i,j,\beta,T)$ is the shift in defect formation energy due to deviations from ideal stoichiometry. The calculation of each term will be described in turn.

1. Harmonic vibrational free energy of defect formation $\Delta\Omega_F^h(i,j,\beta,T)$

First-principles lattice dynamics calculations are especially demanding numerically for the relatively low-symmetry configurations associated with defects. To reduce the computational requirements, we rely on the transferable length-dependent force constant methodology.[21,22] Each chemical bond is characterized by an analytical stiffness-length relationship, whose parameters are fitted to first-principles calculations. The Al–Nb and Ti–Nb parameters were fitted to calculations for titanium aluminide supercells with a Nb substitution, whereas those for the Al–Al, Al–Ti, and Ti–Ti bonds were obtained from supercells without substitutions.[18]

Based on the stiffness-length relationships, the force constants for other atomic configurations (such as supercells

TABLE II. Temperature-dependent contributions to free energy of formation of Nb solutes in TiAl and Ti_3Al at 1075 K (see Sec. III E for details).

Phase	Sublattice	$\Omega_F(0)$	$\Delta\Omega_F^h(T)$	$\Delta\Omega_F^t(T)$	$\Delta\Omega_F^\mu(T)$	$\Delta\Omega_F^{stoi}(T)$	$\Omega_F(T)$
TiAl	Al	−5.568	−0.140	−0.023	0.000	(0)	−5.731
TiAl	Ti	−5.849	−0.030	0.001	−0.052	(0)	−5.929
Ti_3Al	Al	−4.952	−0.093	−0.040	0.000	(0)	−5.084
Ti_3Al	Ti	−6.103	0.072	−0.014	−0.052	0.300	−5.797

with embedded point defects) can be estimated. The resultant force constants are input to a Born–von Kármán lattice dynamics (e.g., Ref. 21) analysis of phonon spectra, in terms of which vibrational free energy within the harmonic approximation is obtained (see the fourth column of Table II).

2. Quasi-harmonic free energy of defect formation $\Delta\Omega_F^h(i,j,\beta,T)+\Delta\Omega_F^t(i,j,\beta,T)$

Thermal expansion may be incorporated into the formulation by considering phonon frequencies to be volume dependent, the so-called quasi-harmonic approximation (e.g., Ref. 21). The equilibrium volume (and the corresponding free energy) at a given temperature is obtained by minimizing the sum of the elastic strain energy of the expanded lattice and the volume-dependent vibrational free energy. The quasi-harmonic treatment yields the sum $\Delta\Omega_F^h(i,j,\beta,T)+\Delta\Omega_F^t(i,j,\beta,T)$, and results listed in the fifth column of Table II for $\Delta\Omega_F^t(i,j,\beta,T)$ are obtained by subtracting the harmonic free energy from the quasiharmonic free energy.

Since the force constants employed in the harmonic calculations are parametrized by bond length, implementation of the quasi-harmonic approximation required no additional force constant calculations. To calculate the elastic energy cost, the bulk moduli of the α_2 and γ phases were fitted to total energy calculations for lattice parameters up to 2% above the equilibrium value. For simplicity, the effect of solutes on the bulk moduli was neglected, as was the slight anisotropy in the thermal expansion of the α_2 and γ phases.

3. Chemical-potential-induced shift $\Delta\Omega_F^\mu(i,j,\beta,T)$

The formation free energies of Nb solutes in the α_2 and γ phases within the two-phase region depend on the host chemical potentials in the temperature range of interest. As mentioned earlier, the chemical potential of Nb is constrained by the assumption of diluteness, but is otherwise arbitrary. For our present purpose, only the temperature dependence of $\mu(\mathrm{Al})-\mu(\mathrm{Ti})$ within the two-phase region is required.

The small deviation of the γ-phase boundary from stoichiometry can be accurately accounted for with a low-temperature expansion[20] based on the antisite energies given in Table I to determine the free energy of the γ phase as a function of Al content. The antisite formation energies were corrected for the effect of lattice vibrations, within the quasi-harmonic approximation, by procedures similar to those outlined above. To model the α_2 phase, whose boundaries deviate markedly from stoichiometry at elevated temperatures, we employ a cluster expansion[29] in conjunction with Monte Carlo simulations. The cluster expansion parameters were fitted to a database generated with first-principles calculations using VASP. These calculations[18] also incorporate lattice vibrational effects, modeled via the transferable force constant scheme and within the quasi-harmonic approximation. Most of the employed codes are incorporated in the ATAT program package.[30]

Using the calculated free energies of the γ and the α_2 phases at $T=1075$ K, we find a two-phase equilibrium at $\mu(\mathrm{Ti})-\mu(\mathrm{Al})=-3.566$ eV; for comparison, $\mu(\mathrm{Ti})-\mu(\mathrm{Al})=-3.513$ eV at $T=0$ K. The effect of this chemical potential shift on the formation free energy is given in the sixth column of Table II.

4. Stoichiometric effect $\Delta\Omega_F^{stoi}(i,j,\beta,T)$

Finally, let us consider the change in the energy of defect formation associated with deviations from the ideal stoichiometries at finite temperatures. In principle, a ternary cluster expansion that incorporates Nb as well as Ti and Al would be useful in this context, but is beyond the scope of the present work, and a more approximate approach was used. Since stoichiometric effects are expected to be most significant for α_2 phase, we will focus on that phase. In the 64-atom cell employed in calculations for the $D0_{19}$ structure, we consider an arrangement with 42 Ti and 22 Al atoms. This composition is close to the observed stoichiometry at high temperatures and can be realized by creating six Al antisite atoms in the ideal $Ti_{48}Al_{16}$ cell used to represent the low-temperature α_2 system. Among the large number of possible arrangements of six antisite Al atoms in the 64-atom cell, we select for computation an arrangement in which the antisite atoms are relatively well separated. For this configuration, prospective sites for substitution on the Ti sublattice may have either zero, one, or two Al antisite atom neighbors, with approximately equal combinatorial weight. Explicit calculations for configurations with either zero or two Al antisite atom neighbors of a Nb solute indicate that $\Delta\Omega_F^{stoi}(i,j,\beta,T)$ is about 0.3 eV for Nb substitution on the Ti sublattice (see the seventh column of Table II). Since Nb favors the Ti sublattice, the stoichiometric correction for the Al sublattice is not calculated.

While this result accounts for the most important energetic contribution to $\Delta\Omega_F^{stoi}(i,j,\beta,T)$, it neglects several higher-order effects. For example, the presence of a Nb impurity may modify the distribution of surrounding Al and Ti atoms. The treatment of such contributions would be feasible with a ternary cluster expansion.

TABLE III. The calculated and experimental values of binary alloy properties for composition $Ti_{1-x}Al_x$. The results of present calculations are listed in the third column. The lattice constants and alloy formation energies (ΔH) are calculated for the ideal stoichiometries [$x_{th}=0.5(0.25)$ for the $\gamma(\alpha_2)$ phase] at zero temperature. The monovacancy formation energies are calculated for off-stoichiometric compositions, as described in the text. The bottom two rows give the phase boundary between the two phase region and the α_2 phase, and between the two phase region and the γ phase. The last column cites references for experimental results.

Phase	Property	Theory	x_{th}	Experiment	x_{expt}	Reference
γ	a (Å)	3.98	0.5	3.98	0.54	VC (Ref. 47)
γ	c (Å)	4.09	0.5	4.07	0.54	VC
α_2	a (Å)	5.75	0.25	5.78	0.28	VC
α_2	c (Å)	4.65	0.25	4.647	0.28	VC
γ	ΔH (eV/at)	−0.414	0.5	−0.378	0.5	KH (Ref. 48)
α_2	ΔH (eV/at)	−0.278	0.25	−0.262	0.25	KH
γ	E_F^V (eV)	1.82,1.91	0.49			
γ	E_F^V (eV)	1.41	0.515	1.41	0.515	B (Ref. 33)
α_2	E_F^V (eV)			1.55	0.29	B
α_2	E_F^V (eV)			1.8	0.229	B
α_2	x_{α_2} ($T=1075$ K)	0.31	0.31	0.35	0.35	O (Ref. 27)
γ	x_γ ($T=1075$ K)	0.47	0.47	0.48	0.48	O

IV. DISCUSSION

A. Intrinsic host material properties

Comparisons of calculated host-material properties with experiment (see Table III) corroborate the accuracy of the LDFT-GGA framework. Such comparisons support our confidence in predictions of solute properties. Comparisons of the predicted solute properties directly with experiment will also be presented; however, such comparisons are more ambiguous than those for the pure host phases.

1. Lattice constants

Predicted lattice constants for the compounds under investigation are generally within 1% of experimental values (cf. Sec. III A) which is typical of the LDFT-GGA. Predicted compound formation energies, ΔH, of TiAl and Ti_3Al overshoot experimental values[31] by about 10%, consistent with earlier first-principles treatments of this property.[17]

2. Point defect energies

Predicted intrinsic-defect energies at zero temperature, assuming ideal stoichiometry, are given in Table I. Experimental values of vacancy formation energies derived from positron annihilation spectroscopy,[32–34] given in Table III, are in the range of 1.55 eV for α_2-$Ti_{77}Al_{23}$ and 1.41 eV for γ-$Ti_{48.5}Al_{51.5}$. The present theoretical predictions are somewhat higher, particularly for Ti_3Al. The discrepancies between the values listed in Table I and experiment are most likely related primarily to the assumptions of ideal stoichiometry and zero temperature.

For the γ phase, however, deviations from stoichiometry are relatively small. Using a lattice gas model[13] and fixing $\mu(\mathrm{Ti})-\mu(\mathrm{Al})=-3.566$ eV at 1075 K, in accordance with results presented in the previous section, we find the γ phase has a composition of $Ti_{50.77}Al_{49.23}$. The corresponding calculated vacancy formation energies on the Al and Ti sublattices are 1.82 and 1.91 eV, respectively. For the composition appropriate to the positron annihilation experiments of Brossmann *et al.*[33] ($Ti_{48.5}Al_{51.5}$), at which vacancies occur predominantly on the Ti sublattice, we predict a Ti vacancy formation energy of 1.41 eV, in excellent agreement with experiment as well as previous first principles calculations[35] (see Table III).

We note, however, that the present analysis does not address the severe electron-density depletion near vacancies that make them stronger perturbations to the host crystal than solute atoms, in general. Accordingly, additional corrections to the LDFT-GGA formulation may be necessary before critical comparisons of calculated vacancy formation free energies with experiment can be made.[36] These complications are not pursued here, however, since our focus is on solutes.

3. Phase boundaries

Phase-boundary compositions of the two-phase region in which the TiAl and Ti_3Al phases coexist may be extracted from the the temperature dependence of the chemical-potential difference $\mu(\mathrm{Al})-\mu(\mathrm{Ti})$ discussed in Sec. III E. The consistency of these predictions with the experimental phase diagram is a significant test. At 1075 K, the predicted phase boundaries are at 31% and 47% Al, respectively, for Ti_3Al and TiAl. The corresponding experimental values[27] are approximately 35% and 48% Al. The TiAl phase boundary is seen to be in good agreement with experiment, and its closeness to the equiatomic limit justifies our application of a low-temperature expansion for this phase. On the other hand, a discrepancy of about 4% appears for the Ti_3Al phase boundary. The precise location of the Ti_3Al phase boundary is highly sensitive to small errors in the calculated free en-

ergies, because the concentration dependence of the free energy of this phase exhibits only weak curvature, which is partly a consequence of the small Al antisite energy (see Table I). Thus, a relatively large error for this phase boundary is perhaps not surprising. A more detailed discussion of the errors inherent in cluster-expansion-based calculations of phase boundaries is given by Ghosh *et al.*[37]

B. Ising-model description of formation energy trends

The trends in the formation energies of substitutional defects in the γ and α_2 phases (cf. Figs. 1 and 2) must follow from trends in such properties as band filling and electronegativity. Rather than attempting to resolve precisely which property is responsible, we explore instead a formulation of total energy based on a nearest-neighbor pseudo-spin Ising model, in which the pseudo-spin represents phenomenologically the variation in the solute chemistry across the periodic table. Within the nearest neighbor Ising model, the energy E of a binary Ti—Al alloy (either the γ or the α_2 phase) is written as

$$E = \mu \sum_i \sigma_i + \sum_{i,j} J_\beta \sigma_i \sigma_j, \tag{12}$$

where the spinlike occupation variables σ_i take the value +1 (Al) or −1 (Ti) depending on the identity of the atom located at site i. The sums are taken, respectively, over all lattice sites i and over all neighboring pairs of lattice sites i,j. The parameter μ is the chemical potential difference $\mu_{\mathrm{Al}} - \mu_{\mathrm{Ti}}$ between Al and Ti within the two-phase region (cf. Sec. III B), while J_β specifies the strength of the interatomic interactions in phase $\beta = \alpha_2$ or γ. For the fcc lattice (associated with the γ phase), the interaction parameter was taken from the nearest neighbor interaction obtained in Ref. 38 ($J_\gamma = 0.064$ eV). For the α_2 phase, the nearest-neighbor interaction parameter was taken from the more accurate thermodynamic model used in Sec. III, with in-layer and out-of-layer interactions on the hexagonal lattice averaged ($J_{\alpha_2} = 0.045$ eV). Although the parameters μ, J_{α_2}, and J_γ are not all independent within a nearest-neighbor model, we treat μ as an adjustable parameter because of its sensitivity to the long-range interactions neglected in the Ising model.

The Ising Hamiltonian, Eq. (12), can be extended in a formal way to multicomponent systems by including additional parameters;[29] however, a simpler treatment is adopted here. Since Ti and Al almost bracket the range of the periodic table in which the transition elements reside, it is reasonable, from a heuristic viewpoint, to characterize the chemical behavior of a given transition element via a linear interpolation between Ti and Al, in terms of the periodic table column, c. Accordingly, solute atoms are assigned a pseudo-spin $\sigma_i = -1 + 2(c-4)/9$, which reduces to −1 for Ti and +1 for Al. These fractional pseudo-spin variables are then used in conjunction with Eq. (12) to predict the properties plotted in Figs. 1 and 2. The calculation of these defect formation energy differences is performed in the dilute limit by considering a single isolated impurity, and the detailed impurity distribution therefore need not be specified. The adjustable parameter μ was set to match the crossing of the horizontal axis of the TiAl data in Fig. 1. The resultant value, $\mu = -0.38$ eV/atom, is within 25% of the value obtained directly from the nearest-neighbor model (−0.51 eV/atom). The model predictions, analogous to the first-principles calculations plotted in Figs. 1 and 2, are shown in Figs. 4(a) and 4(b).

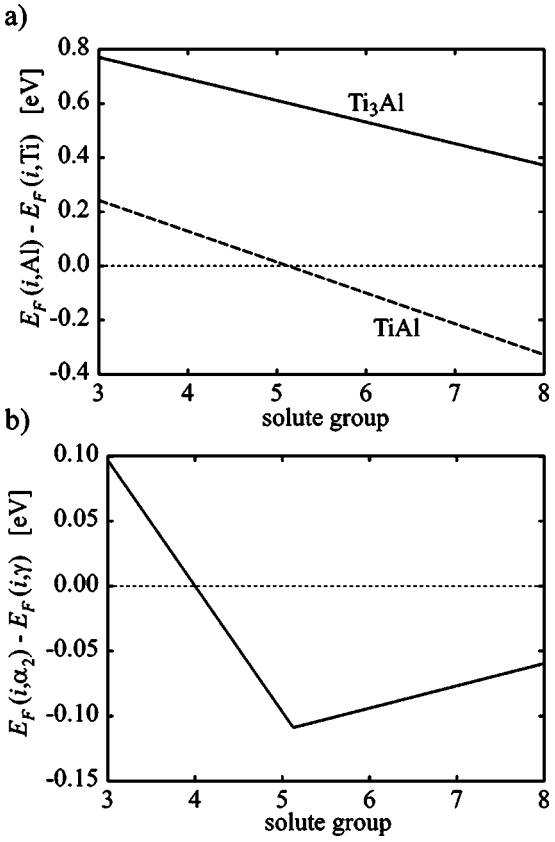

FIG. 4. The predictions of solute formation energies based on simplified Ising model, Eq. (12). Panel (a) is to be compared with Fig. 1 and panel (b) with Fig. 2.

The Ising model captures the most salient features of the trends observed in the formation energies calculated with first-principles methods. First, as seen in Figs. 1 and 4(a), transition-metal solutes always prefer the Ti sublattice of the Ti_3Al phase, while, for the TiAl phase, the solute preference shifts from the Ti to the Al sublattice as the transition series is traversed. Second, as seen in Figs. 2 and 4(b), solutes tend to prefer the α_2 phase, particularly in the middle of a transition element series. Further insight into this behavior can be gained by recognizing that Ti–Al is an ordering system for which it is favorable to maximize the number of "unlike" bonds (i.e., nearest-neighbor bonds between distinct chemical species). Ti sites in ordered stoichiometric Ti_3Al, with eight like and four unlike nearest neighbors, would prefer more unlike neighbors, which can be achieved by substitution of atoms with $\sigma_i > -1$ on the Ti sublattice. Solute substitution on the Al sublattice, whose sites already have all unlike neighbors, confers no such advantage, and substitution on the Ti sublattice of the Ti_3Al phase is therefore preferred. Ordered $L1_0$ TiAl has the maximum number (eight) of unlike bonds possible on an fcc lattice, so that solutes with

values of σ_i intermediate between those of Ti and Al effectively decrease the number of unlike bonds. The energy cost of substitution is minimized when the more "aluminumlike" solutes (i.e., with larger c) reside on the Al sublattice, and the more "titaniumlike" solutes (i.e., with smaller c) reside on the Ti sublattice. This switch in preference is at the origin of the sign change in Figs. 1 and 4(a) and also explains the presence of a minimum in the middle of the transition metal sequence in Figs. 2 and 4(b), where substitutions on either sublattice of the $L1_0$ structure are relatively unfavorable.

We have seen that the Ising model predictions, based on one adjustable parameter, are consistent with the most significant features of the trends exhibited in Figs. 1 and 2. The correspondence between the first-principles calculations and the Ising model is, of course, not exact in all details [for example, the best fit line to results for Ti_3Al in Fig. 1 appears horizontal, whereas the line in Fig. 4(a) shows a small negative slope]. Extensions of the Ising model would presumably bring the model and the first-principles results into closer correspondence.

C. Solute sublattice preference in the γ phase

The sublattice partitioning of ternary elements in a binary host can be determined experimentally by the atom-location-channeling-enhanced-microanalysis technique (ALCHEMI),[39] statistical ALCHEMI,[40] as well as by atom-probe field ion microscopy[41] and x-ray diffraction.[42] Ideally, ALCHEMI yields the fraction f_{Ti} (or f_{Al}) of a given solute species on the Ti (or Al) sublattice. For large values of ΔE_F (Fig. 1) we can approximate

$$1/f_{\mathrm{Ti}} = 1 + w \exp[\Delta E_F(i,T)], \tag{13}$$

where w is the ratio of Ti to Al atoms in the stoichiometric compounds, if deviations of the host phase from ideal stoichiometry, and the consequent antisite host-atom populations, may be ignored. Although this approximation may be justified for γ-TiAl in some cases, it is unlikely to be accurate for the α_2 phase. For single-phase γ-TiAl, a lattice gas model was developed to predict the fractional site occupancy for a given composition and temperature[13] when ΔE_F is small. For comparison with experiment, we perform calculations for a nominal composition of $(Ti_{51}—Al_{49})_{99}-M_1$, where M is the ternary element, which is close to the boundary of the binary $\alpha_2+\gamma$ phase field for temperatures in the range 800–1473 K.[43]

Results for the various ternary additions are plotted in Fig. 5 together with the statistical ALCHEMI results of Rossouw *et al.*[40] The crossover that occurs between predominant Ti sublattice occupancy of early transition elements and predominant Al sublattice occupancy of late transition elements is clear in both theory and experiment. The plotted results are in close agreement with previous LDFT calculations on a smaller set of solutes.[13] We note that in both Fig. 5 and Fig. 6, discussed below, a larger discrepancy appears for Mn than for most other solutes. The results for Mn were not significantly changed by including spin polarization. A higher-level approximation than LDFT-GGA may be required to achieve greater accuracy for Mn.

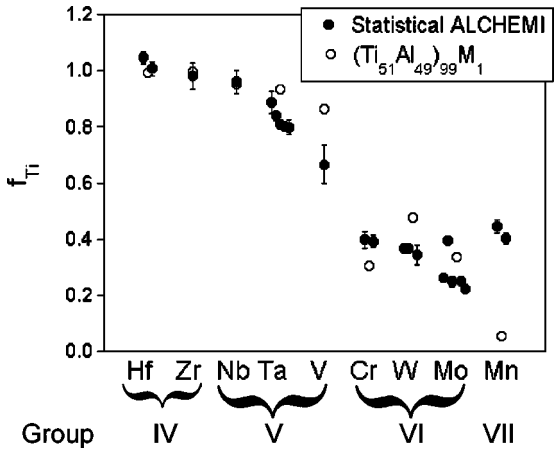

FIG. 5. The predicted (open circles) and measured (filled circles) partitioning of transition-metal solutes in γ-TiAl with composition $(Ti_{51}Al_{49})_{99}M_1$ at 1473 K. The ordinate represents the fraction of solutes that reside on the Ti sublattice.

D. Solute partitioning: Experiment

The ratio of solute concentration in TiAl to that in Ti_3Al may be written

$$c(i,j,\alpha_2,T)/c(i,j,\gamma,T) = w_p \exp[\Delta E_F^{\alpha_2\gamma}(i)], \tag{14}$$

assuming ideal stoichiometries, where w_p is the sublattice factor. For stoichiometric Ti_3Al and TiAl, the sublattice factor $w_p=2/3$, if the solutes in Ti_3Al are assumed to reside on the Ti sublattice, as suggested by the results in Fig. 1. For an α_2-phase stoichiometry close to Ti_2Al, a slightly larger sublattice factor would be appropriate. In Fig. 6, numerical results for transition metal solutes are plotted, using $w_p=1$, along with experimental results given by Rossouw *et al.*[40]

Both ALCHEMI measurements[40] and three-dimensional atom probe microscopy observations[44,45] indicate that Zr and Nb prefer the γ phase, whereas other transition-metal solutes

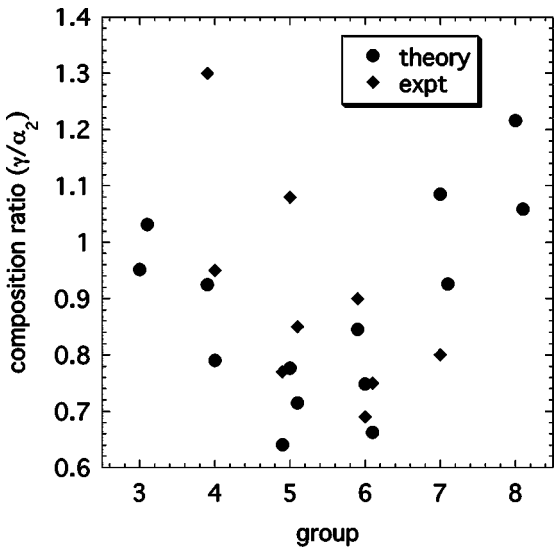

FIG. 6. Predicted (filled circles) and measured (diamonds) ratio of solute concentration in the γ phase to that in the α_2 phase.

(Hf, Cr, Ta, Mn, V, W, and Mo) preferentially partition to the α_2 phase. Thus, an apparent discrepancy exists between experiment and the zero-temperature predictions shown in Fig. 2, in which both Nb and Zr exhibit lower formation energies in Ti_3Al than TiAl, by 0.25 and 0.08 eV, respectively. We now consider whether elevated-temperature corrections are sufficiently large to reverse the sign of the formation energy difference between the phases.

E. Temperature-dependent contributions to formation free energies

In Sec. III E, several types of temperature-dependent contributions to the solute formation free energies were calculated for Nb at a reference temperature of 1075 K (see Table II). We consider the dilute limit, and the quantities $\Omega_F(i,j,\beta,0)$ and $\Omega_F(i,j,\beta,T)$ in Table II therefore do not reflect contributions associated with the Nb chemical potential, as mentioned previously.

The temperature corrections due to lattice vibrations, thermal expansion, and host-chemical-potential shift (columns 4–6 in Table II) are fairly small and do not reverse the zero-temperature preference for the Ti sublattice of the α_2 phase; however, the correction due to the deviation of the Ti_3Al phase from ideal stoichiometry (seventh column) is relatively larger. This term was estimated only for the Ti sublattice, which is preferred by Nb in each phase (cf. Fig. 1). Comparing the results in the first and last columns of the table, the formation energy difference $\Omega_F(\mathrm{Nb},(\mathrm{Ti}),\alpha_2,T) - \Omega_F(\mathrm{Nb},\mathrm{Ti},\gamma,T)$ is seen to shift from -0.254 at 0 K to 0.133 at 1075 K, indicating that temperature corrections do appear to reverse the Nb solute phase preference from α_2 at zero temperature to γ at 1075 K. Our predictions at 1075 K are therefore consistent with experimental observation. Although numerical calculations of the temperature-dependent shift in formation energies were not performed for solutes other than Nb, it is reasonable to expect the sign of the shift to be the same for most solutes. Therefore, we anticipate that similar calculations to those for Nb would show that the sign of $E_F(\mathrm{Nb},\alpha_2) - E_F(\mathrm{Nb},\gamma)$ for Zr shifts to positive values at elevated temperatures, in accord with experiment.

F. Solute formation energies in carbides

One of the motivations for this work was to identify solutes that segregate to carbide precipitates, or their interfaces with the host matrix, and consequently enhance their stability against coarsening. The trends exhibited by the results plotted in Fig. 3 suggest that the early (groups IIIB and IVB) transition metals are the best candidates for such segregation, although even for these early transition elements, the zero-temperature calculations yield formation energies higher in the carbide than in the matrix for all solutes except Y. Ta favors the carbide over TiAl, but not over Ti_3Al. In most of these comparisons, the solute formation energy in the H-type carbide was employed; transition-metal solutes have a lower formation energy in the H-type than the P-type carbide, with Sc the sole exception. Zr showed essentially identical formation energies in H- and P-type carbides.

Based on these results, Y would appear to be the best candidate for a solute that partitions to carbide precipitates. Rossouw *et al.*,[40] however, note that Y, as well as La, exhibits negligible solute solubility in the host, but instead forms Al_2X precipitates. In (zero-temperature) simulations, we find that Y does show a strong attraction for $Ti_2AlC/TiAl$ interfaces,[46] and Y migration to such interfaces therefore remains a possibility.

Overall, the present simulations do not suggest a strong candidate for segregation to carbide precipitates, although when effects of temperature and stoichiometry, which are excluded from our calculations, as well as interactions with carbide-host interfaces are taken into account, different behavior may emerge.

V. SUMMARY AND CONCLUSIONS

Formation energy calculations for dilute substitutional solutes in TiAl and Ti_3Al, as well as in the H- and P-type carbide precipitates, have been performed with first-principles methods, using the VASP code. The selected solutes include transition metals from the three transition periods, and nontransition elements B and Si, which represents virtually the entire set of dopants that are commonly used in Ti–Al alloys. Most of the calculations correspond to zero temperature, but corrections to the solute formation free energy appropriate to 800 °C were calculated in the case of Nb dopants. One source of corrections to Ω_F larger than k_BT in absolute magnitude is associated with the stoichiometry shift of the α_2 phase at elevated temperatures. Other corrections of the order of k_BT are identified. Although the corrections to formation free energies at 800 °C are of the order of tenths of an eV, and therefore not insignificant, the main trends exhibited by the zero-temperature solute formation energies as a function of periodic table group (or number of outer-shell electrons) appear to be borne out in experiments that measure atomic configurations representative of high temperatures. The experimental probes that provide the most critical tests of our calculations are the Statistical ALCHEMI method[40] and three-dimensional atom-probe microscopy.[44,45]

Our calculations indicate that all transition metal solutes prefer the Ti sublattice of Ti_3Al. In TiAl, however, the preference of early transition-metal groups for the Ti sublattice crosses over to a preference for the Al sublattice by later transition groups. The zero-temperature calculations predict the crossover to occur in the vicinity of groups V and VI, which is roughly consistent with experiment.

Our calculations predict that the solutes in the middle of the transition series partition strongly to Ti_3Al, whereas those at either end partition roughly equally between the two phases, or slightly favor TiAl. Experiment agrees with this overall trend, but shows discrepancies for individual solutes, such as Nb, which may be removed with the inclusion of thermal corrections to the solute formation free energy.

The zero-temperature formation energy calculations do not identify any solute that would be likely to partition to carbide precipitates. The best prospects for such partitioning, however, are group IIIB and IVB elements.

ACKNOWLEDGMENTS

Research at Northwestern University was supported by U. S. Department of Energy Grant Nos. DE-FG02-96ER45597 (RB, SG and DNS) and DE-FG02-01ER45910 (AVDW and MA). CW was supported by the Air Force Office of Scientific Research at the U. S. Air Force Research Laboratory, Materials and Manufacturing Directorate, Wright Patterson AFB under Contract No. F33615-96-C-5258. A grant of computer time at the National Energy Research Computer Center at Lawrence Berkeley Laboratory is gratefully acknowledged. This work was also supported in part by a grant of computer time from the DoD High Performance Computing Modernization Program, at the Aeronautical Systems Center-Major Shared Resource Center, on the IBM-SP3. This project benefited from computing resources provided by the National Partnership for Advanced Computational Infrastructure at the University of Michigan.

APPENDIX: DILUTE-SOLUTE LIMIT FOR NONSTOICHIOMETRIC INTERMETALLIC COMPOUNDS

The relationship between the solute concentration in the dilute limit and the solute formation energy in a nonstoichiometric binary host system is formulated in this Appendix. Consideration of the dilute limit enables a low-temperature expansion of the solute partition function, which leads to formal simplification.

Let σ denote a particular atomic arrangement of binary alloy phase β with free energy $\Omega(\sigma,\beta,T)$ and τ an arrangement of solutes (i.e., impurities) on the lattice with free energy $\Omega(\tau,\sigma,\beta,T)$. $\Omega(\sigma,\beta,T)$ represents the free energy of a system constrained to be in configuration σ and phase β, and thus contains all free energy contributions other than that of configurational entropy. The partition function of a system of N atoms can then be expressed as

$$Z = \sum_{\tau} m_{\tau}^{-1} \sum_{\sigma} \exp[-\Omega(\tau,\sigma,\beta,T)/(k_B T)], \tag{A1}$$

where $m_\tau = 2^{Nc_i}$, the number of distinct binary configurations σ that may be transformed to the configuration τ when the Nc_i solutes replace the appropriate host atoms on the lattice of phase β. A factored form of the partition function,

$$Z = Z_B Z_I, \tag{A2}$$

where

$$Z_B = \sum_{\sigma} \exp[-\Omega(\sigma,\beta,T)/(k_B T)], \tag{A3}$$

and

$$Z_I = \sum_{\tau} \exp[-\bar{\Omega}_F(\tau,\beta,T)/(k_B T)], \tag{A4}$$

in terms of the partition functions of the binary and of the solute systems, can be obtained by standard manipulations. The effective formation energy for solute configuration τ may be expressed as

$$\bar{\Omega}_F(\tau,\beta,T) = -k_B T \ln\left(Z_B^{-1} \sum_{\sigma} \exp\{[-\Omega(\sigma,\beta,T) - U_F(\tau,\sigma,\beta,T)]/(k_B T)\}\right), \tag{A5}$$

where we have introduced a solute configurational energy

$$U_F(\tau,\sigma,\beta,T) = \Omega(\tau,\sigma,\beta,T) + k_B T \ln m_\tau - \Omega(\sigma,\beta,T). \tag{A6}$$

$\bar{\Omega}_F(\tau,\beta,T)$ is a thermodynamic average of U_F over binary configurations σ.

We note that the difference in free energies $\Omega(\tau,\sigma,\beta,T) - \Omega(\sigma,\beta,T)$ contains a term $-\mu_i N c_i$, where μ_i is the chemical potential of the ternary solute species; in the above definition of the defect formation free energy, the term $Nc_i k_B T \ln 2$ can thus be viewed as a correction to μ_i that results from the deviation of the reference state alloy composition from the ideal stoichiometry, when a low-temperature expansion is performed for the solutes. This shift in the chemical potential, however, is of little significance in the present work, since the value of μ_i is constrained to be consistent with the chosen solute concentration. This shift would be important in calculations of the solute solubility limit using a common tangent construction involving the formation free energies of precipitate phases.

A consequence of Eq. (A2) is that thermodynamic quantities can be expressed as a sum of binary alloy and (ternary) solute contributions. When c_i is sufficiently dilute to warrant a first-order low-temperature expansion of Z_I, the grand potential

$$\Omega = \Omega_B - (N/\nu) k_B T \sum_{j} \exp[-\Omega_F(i,j,\beta,T)/(k_B T)], \tag{A7}$$

where ν is the number of sites per unit cell and N/ν is the number of unit cells in the lattice, $\Omega_B = -k_B T \ln Z_B$ is the grand potential of the binary system, and

$$\Omega_F(i,j,\beta,T) \equiv \bar{\Omega}_F(\tau_{ij},\beta,T) \tag{A8}$$

is the effective (configurationally averaged) formation free energy of a single solute i on sublattice j, an arrangement we denote as τ_{ij}. [The summation over j in Eq. (A7) runs over all sites in a unit cell that belong to the sublattice in question. More formally, this could be written as a sum over k, where j_k denotes an individual site in the unit cell basis that belongs to sublattice j.] We note that the defect (solute) contributions to the grand potential from formation energy and configurational entropy are not readily separable, as they are in thermodynamic formulations based on the Gibbs free energy, and Eq. (A7) is therefore not intuitively obvious.

Equation (2) in the main text can be obtained essentially by differentiation with respect to the solute chemical potential, $c_i = \partial\Omega/\partial\mu_i$, with the host chemical potentials held constant. Formally, however, the sublattice concentrations must be considered separately. Thus, differentiation with respect to $\mu_{i,j}$ picks out one term in the sum. To calculate such sublattice-specific compositions, it is necessary to introduce

a fictitious site-specific chemical potential $\mu_{i,j}$ for species i on sublattice j. After differentiation with respect to $\mu_{i,j}$, one can set $\mu_{i,j}=\mu_i$, the solute chemical potential for the system. Equation (2) is thus shown to hold for the case of dilute ternary additions to binary compounds with arbitrary composition, provided the defect formation free energy is defined formally as above. This formulation is applicable to the γ and α_2 Ti–Al alloy phases, in both of which the nonstoichiometric compositions are accommodated by antisite disorder. Explicit evaluation of the configurational averages that occur in the generalized formation energy $\overline{\Omega}_F$, of course, may be tedious.

[1] F. Appel and R. Wagner, Mater. Sci. Eng., R. **22**, 187 (1998).
[2] E. A. Loria, Intermetallics **9**, 997 (2001).
[3] J. C. Tang, B. Y. Huang, W. S. Liu, Y. H. He, K. C. Zhou, A. H. Wu, K. Peng, W. Qin, and Y. W. Du, Mater. Res. Bull. **38**, 2018 (2003).
[4] B. D. Worth, J. W. Jones, and J. E. Allison, Metall. Mater. Trans. A **26A**, 2947 (1995).
[5] T. A. Parthasarathy, M. G. Mendiratta, and D. M. Dimiduk, Scr. Mater. **37**, 315 (1997).
[6] Z. D. Xiang, S. R. Rose, and P. K. Datta, Mater. Sci. Technol. **19**, 1247 (2003).
[7] X. H. Wu, D. Hu, and M. H. Loretto, J. Mater. Sci. **39**, 3935 (2004).
[8] T. Haruna, T. Iwata, T. Sundararajan, and T. Shibata, Mater. Sci. Eng., A **329**, spec. SI, 745 (2002).
[9] J. C. Zhao and J. H. Westbrook, MRS Bull. **28**, 622 (2003).
[10] W. H. Tian, T. Sano, and M. Nemoto, Philos. Mag. A **68**, 965 (1993).
[11] M. Karadge, Y. W. Kim, and P. I. Gouma, Metall. Mater. Trans. A **34A**, 2129 (2003).
[12] R. Benedek, D. N. Seidman, and C. Woodward, Interface Sci. **12**, 57 (2004).
[13] C. Woodward, S. Kajihara, and L. H. Yang, Phys. Rev. B **57**, 13 459 (1998).
[14] Y. Mishin and D. Farkas, Philos. Mag. A **75**, 169 (1997).
[15] M. Hagen and M. Finnis, Mater. Sci. Forum **207–209**, 245 (1996).
[16] C. L. Fu, Y. Y. Ye, M. H. Yoo, and K. M. Ho, Phys. Rev. B **48**, 6712 (1993).
[17] M. Asta, D. de Fontaine, and M. van Schilfgaarde, J. Mater. Res. **8**, 2554 (1993).
[18] A. van de Walle and M. Asta (unpublished).
[19] W. J. Zhang and F. Appel, Mater. Sci. Eng., A **329**, spec. SI, 649 (2002).
[20] C. Woodward, M. Asta, G. Kresse, and J. Hafner, Phys. Rev. B **63**, 094103 (2001).
[21] A. van de Walle and G. Ceder, Rev. Mod. Phys. **74**, 11 (2002).
[22] E. Wu, G. Ceder, and A. van de Walle, Phys. Rev. B **67**, 134103 (2003).
[23] Y. Wang and J. P. Perdew, Phys. Rev. B **44**, 13 298 (1991).
[24] G. Kresse and J. Furthmüller, Comput. Mater. Sci. **6**, 15 (1996); Phys. Rev. B **54**, 11 169 (1996).
[25] D. Vanderbilt, Phys. Rev. B **41**, 7892 (1990).
[26] H. J. Monkhorst and J. D. Pack, Phys. Rev. B **13**, 5188 (1976).
[27] I. Ohnuma, Y. Fujita, H. Mitsui, K. Ishikawa, R. Kainuma, and K. Ishida, Acta Mater. **48**, 3113 (2000).
[28] C. G. Van de Walle, D. B. Laks, G. F. Neumark, and S. T. Pantelides, Phys. Rev. B **47**, 9425 (1993).
[29] J. M. Sanchez, F. Ducastelle, and D. Gratias, Physica A **128**, 334 (1984).
[30] Alloy Theoretic Automated Toolkit (ATAT), a collection of alloy theory codes developed by A. van de Walle. See http://cms.northwestern.edu/atat/; A. van de Walle, M. Asta, and G. Ceder, CALPHAD: Comput. Coupling Phase Diagrams Thermochem. **26**, 539 (2002).
[31] R. R. Zope and Y. Mishin, Phys. Rev. B **68**, 024102 (2003).
[32] H. E. Schaefer and K. Badura-Gegen, Defect Diffus. Forum **A143–147**, 193 (1997).
[33] U. Brossmann, R. Würschum, K. Badura, and H. E. Schaefer, Phys. Rev. B **49**, 6457 (1994).
[34] R. Würschum, E. A. Kümmerle, K. B. Gergen, A. Seeger, C. Herzig, and H. E. Schaefer, J. Appl. Phys. **80**, 724 (1996).
[35] C. Woodward and S. Kajihara, Acta Mater. **47**, 3793 (1999).
[36] T. R. Mattsson and A. E. Mattsson, Phys. Rev. B **66**, 214110 (2002).
[37] G. Ghosh, M. Asta, and G. B. Olson, CALPHAD: Comput. Coupling Phase Diagrams Thermochem. **26**, 49 (2002).
[38] A. van de Walle and G. Ceder, J. Phase Equilib. **23**, 348 (2002).
[39] Y. L. Hao, D. S. Xu, Y. Y. Cui, R. Yang, and D. Li, Acta Mater. **47**, 1129 (1999).
[40] C. J. Rossouw, C. T. Forwood, M. A. Gibson, and P. R. Miller, Philos. Mag. A **74**, 57 (1996); **74**, 77 (1996).
[41] J. Wesemann, W. Falecki, and G. Frommeyer, Phys. Status Solidi A **177**, 319 (2000).
[42] S. Kim, D. Nguyen-Manh, G. D. W. Smith, and D. G. Pettifor, Philos. Mag. A **80**, 2489 (2000).
[43] F. Zhang, S.-L. Chen, and Y. A. Chang, in *Gamma Titanium Aluminides*, edited by Y.-W. Kim, R. Wagner, and M. Yamaguchi (The Minerals, Metals and Materials Society, Pittsburgh, 1995), p. 131.
[44] D. J. Larson and M. K. Miller, Mater. Charact. **44**, 159 (2000).
[45] S. S. A. Gerstl, Y. W. Kim, and D. N. Seidman, Interface Sci. **12**, 303 (2004).
[46] R. Benedek (unpublished).
[47] P. Villars and L. D. Calvert, *Pearsons Handbook of Crystallographic Data for Intermetallic Phases* (ASM, Materials Park, OH, 1991).
[48] O. Kubaschewski and G. Heymer, Trans. Faraday Soc. **56**, 473 (1960).